03 Sep 2020

New Experimental Apparatus to Investigate Hot Tearing Behavior in Steel

Yanru Lu

Laura Bartlett
Missouri University of Science and Technology, lnmkvf@mst.edu

Ronald J. O'Malley
Missouri University of Science and Technology, omalleyr@mst.edu

Semen Naumovich Lekakh
Missouri University of Science and Technology, lekakhs@mst.edu

et. al. For a complete list of authors, see https://scholarsmine.mst.edu/matsci_eng_facwork/2698

Recommended Citation

Y. Lu et al., "New Experimental Apparatus to Investigate Hot Tearing Behavior in Steel," *Proceedings of the AISTech 2020 (2020, Cleveland, OH)*, pp. 1460-1469, Association for Iron & Steel Technology (AIST), Sep 2020.
The definitive version is available at https://doi.org/10.33313/380/157

DOI 10.33313/380/157

New Experimental Apparatus to Investigate Hot Tearing Behavior in Steel

Yanru Lu, Laura N. Bartlett, Ronald J. O'Malley, Simon N. Lekakh, Mario F. Buchely

Peaslee Steel Manufacturing Research Center, Department of Materials Science and Engineering
Missouri University of Science and Technology
1400 N Bishop Avenue, Rolla, MO, USA, 65409-0340
Phone: 573-341-4711
Email: lnmkvf@mst.edu

ABSTRACT

Hot tearing is a complex thermomechanical phenomenon occurring in the semi-solid region. Strain in this region can induce cracking and localized alloying element segregation. An apparatus for investigating hot tearing was developed utilizing a servo-motor controlled cylinder to apply a pre-determined amount of strain to the solidifying shell. A special mold was developed using filling and solidification modeling to ensure that dendrite growth was perpendicular to applied strain. A computer-automated system was utilized to control the strain and strain rate and measure the force and displacement. Solidification experiments utilizing AISI 1020 steel validated the apparatus capabilities and optimized testing parameters.

Keywords: Hot Tearing, Strain and Strain Rate, Directional Solidification

INTRODUCTION

Hot tearing is a common irreversible defect that usually appears as cracks, segregation or fractures in the mushy zone during solidification of steel. It occurs when a casting is strained to failure in the semi-solid region during solidification and can lead to alloy and impurity element segregation, porosity formation, and precipitation of inclusions [1-2]. These defects can be accentuated by poor caster alignment and damaged support rolls, as well as non-uniform cooling [3- 4] and soft cooling that can induce shell bulging. During solidification, the existence of residual low melting point liquid results in reduced ductility and increased susceptibility to cracking. This can be magnified by a coarse columnar grain structure, entrapped porosity, and segregation of alloying elements and impurities like Mn, C, Si, S, P [5]. As shown in Figure 1, the ductility of the solidifying steel shell remains almost zero as long as a liquid film exists between the dendrites [6]. Therefore, if there is sufficient strain that is perpendicular to the direction of dendrite growth, a hot tear can be generated.

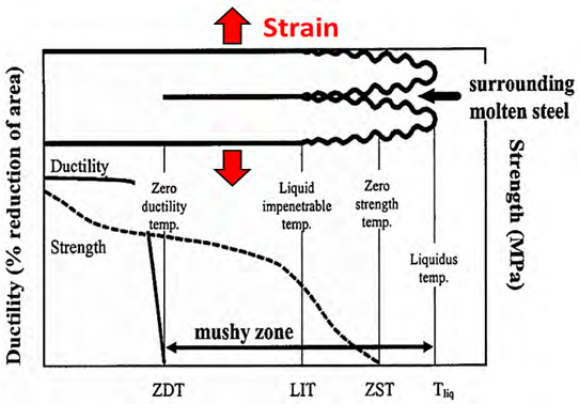

Figure 1: Schematic diagram of mechanical properties in the mushy zone during continuous casting of steels [6].

The ability to understand and predict the casting conditions that cause hot tearing is important to steel mills and foundries for process design, quality control, and development of new steel grades. Hot tearing has been studied for decades [7-8]. However, the effects of segregation of alloying elements such as C, Mn, Al, Si, and S etc. on hot tearing sensitivity are still not well known. This often makes it difficult to predict the hot tearing susceptibility for new steel grades. Over the years, researchers have developed many different experimental tools to investigate hot tearing. Some of these methods employ different constraint conditions to induce stress or strain on the solidifying solid shell to promote the formation of hot tearing [9-12]. Wang et al. [13] used a ring mold to study the hot tearing susceptibility of Mg alloys. The constrained rod casting (CRC) approach has also been used by several researchers and consists of rod shaped castings with different lengths or diameters, as shown schematically in Figure 2 [14-15]. Stress is introduced by constraining shrinkage of the solidifying casting to initiate hot tearing in the area that experiences the maximum stress, such as the conjunction area of the round cap and the column in Figure 2 (a). These CRC experimental methods have been widely used to determine hot tearing sensitivity of both Mg and Al alloys in permanent molds, as summarized by J. Song and coworkers [7]. However, both of these methods are qualitative and do not provide a quantitative measure of critical stress or strain for hot tearing.

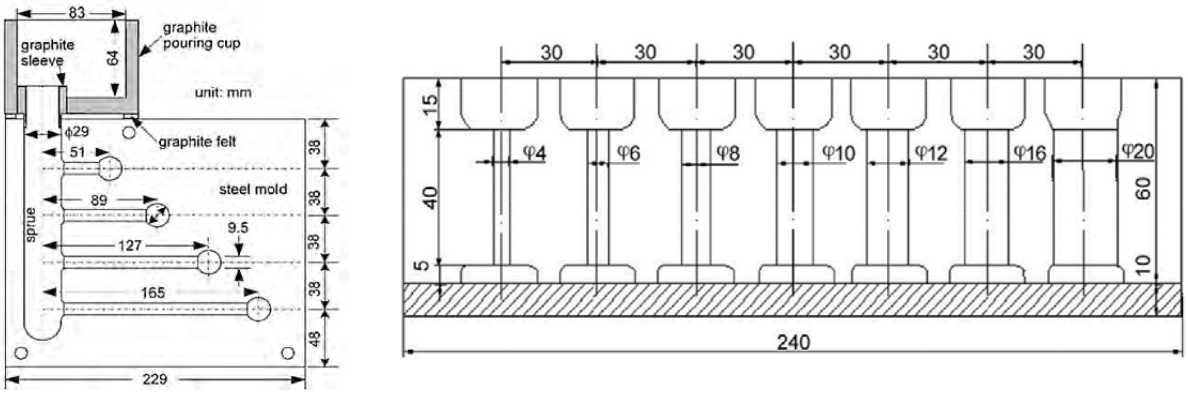

(a) (b)

Figure 2: Schematic of different designs of constrained rod castings used to determine hot tearing sensitivity in aluminum and magnesium castings: (a) a design that varies the rod length [14] and (b) a design that varies the rod diameter [15].

Fewer experimental methods have been designed to study the hot tearing susceptibility of steels. One of the most widely used tests is the constrained T-shaped casting. Monroe and Beckermann [16] used a T section setup with a force and displacement measurement devices to quantitatively study the hot tearing behavior of low carbon low alloy steels. The measured force and displacement in this approach were in good agreement with their simulated force and displacement, respectively. However, the relationship between their measured data with the critical stress or critical strain was not discussed in their work. Bhiogade et al. [17] used the constrained T-shaped casting to study hot tearing susceptibility of a stainless steel and showed that strain and strain rate are more critical for hot tearing than stress. All of the proceeding constrained casting testing approaches share a common drawback; they all rely on solidification shrinkage contraction to develop the strain to form hot tearing. In addition, the amount of contraction and the hot tearing susceptibility will vary as a function of steel composition, which makes it difficult to compare the hot tearing susceptibility for different steel grades at a consistent level of strain.

In recent studies, the submerged split-chill tensile (SSCT) test was developed by Ackermann et al. and applied by Hiebler and other researchers [18-20] to apply controlled deformation to the solidifying steel shell. As shown in Figure 3, a solid cooper or steel test body, which can be split into two halves, was submerged into the liquid steel. After a shell of sufficient thickness has formed around the test body, the lower part was moved downwards at a controlled velocity. The force and displacement were recorded during the test. This method allows researchers to study the mechanical behavior of the solidifying steel shell and investigate the relationship between the hot tearing susceptibility and process parameters encountered in the continuous casting process. However, the experiment setup for this test involves immersion of a water cooled copper or steel test body into molten steel contained in an induction furnace. Therefore, this experiment must be extremely well designed for the safety of the operation and to protect the testing devices from high temperature.

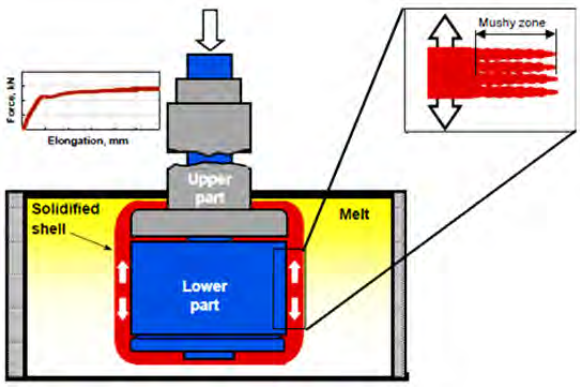

Figure 3: Schematic diagram of the SSCT test method.

To study the hot tearing behavior for different steel grades, a novel approach was developed that overcomes these shortcomings and provides a repeatable and quantitative method of measuring hot tearing susceptibility at controllable strain rates for applications in the continuous casting process.

EXPERIMENTAL PROCEDURE

The Controlled Deformation Test (CDT) was developed in the current study to investigate hot tearing in a quantitative way in a solidifying casting. To apply a controlled strain to the mushy zone (see Figure 1) and develop test conditions that are comparable with the continuous casting process, the dendrite growth direction in the solidifying area of casting should be perpendicular to the direction of the applied strain and the solid shell growth in that area should be uniform. Figure 4 shows a schematic of the continuous casting process and highlights the dendritic nature of the expected shell growth. The experimental conditions of the CDT were designed to produce uniform shell growth in a cylindrical casting in which controlled amounts of deformation could be induced on the shell to replicate strains encountered in continuous casting.

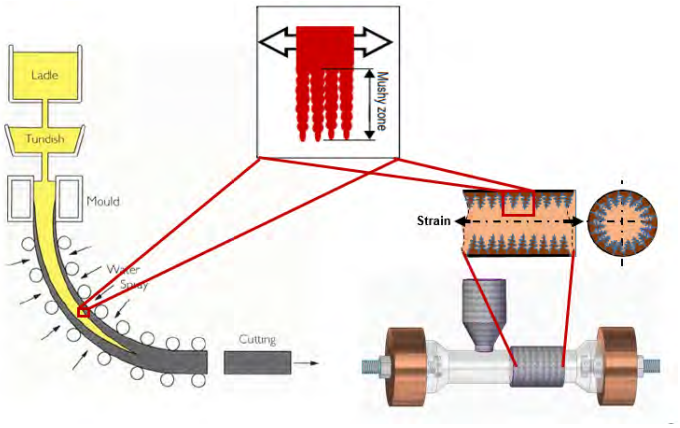

Figure 4: Similarity of the solidification patterns in the continuous casting process and the proposed testing method.

Casting and mold design

A resin bonded, silica sand mold was designed to provide directional solidification and a uniform shell growth in the cylindrical, tensile-bar shaped casting, as shown in Figure 5. A low thermal conductivity insulation sleeve was imbedded into the no-bake sand mold to delay solidification in the test area. The pouring cup also served as a large central riser to ensure proper feeding of the casting during solidification. Two water cooled copper chills were used in the mold to freeze the ends of the bar casting in order to allow transfer of the computer controlled linear displacement to the partial shell in the insulation sleeve area, as shown in Figure 5. The diameter of the reduced section of the casting is 50 mm, and the total length of the casting is 280 mm.

To examine the solidification pattern and evaluate the uniformity of solid shell growth in the insulation sleeve area, filling and solidification software MAGMASOFT (Version 5.3) was used to simulate the solidification process and determine testing temperature.

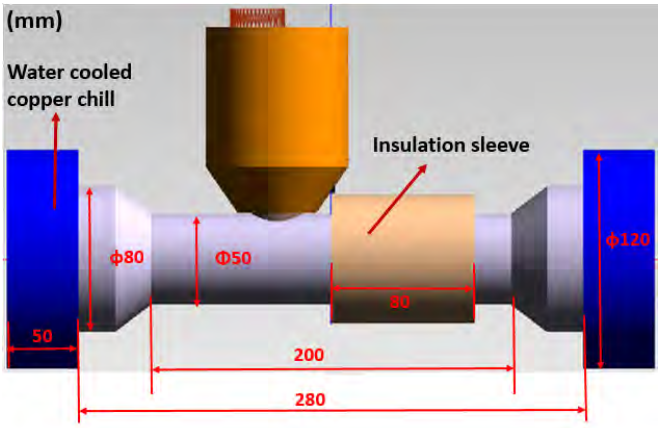

Figure 5: Side view of the test casting design showing the cylindrical test casting, insulation sleeve used to delay solidification in the test area, and water cooled copper chills on each side of the casting used to induce solidification and allow mechanical locking of the test casting.

Test apparatus

A schematic of the CDT apparatus is shown in Figure 6 (a). The test was designed to control displacement with high precision and measure the resultant displacement and force on the solidifying shell as a function of time. Thus, it is possible to apply a certain amount of strain to the solidifying solid shell at a controlled strain rate. The experimental setup consists of an electric cylinder, which was powered by a servo motor and controlled by an electric drive. Rotational movement of servomotor was translated to reciprocate linear movement using high gear ratio electric cylinder. A 20KN compression & tension load cell and a 25mm linear variable differential transformer (LVDT) were used to control and monitor force and displacement as a function of time. Copper chills were water cooled to intensify solidification and protect heating the load cell. A threaded steel rod, with two clamping nuts on the end, penetrates the copper chills and protrudes on both sides into the casting cavity, as shown in the detailed view in Figure 6 (b). At the left side, the threaded rod was fixed to the platform, and at the right side, the threaded rod was connected to the load cell (and electric cylinder) by a flange coupling.

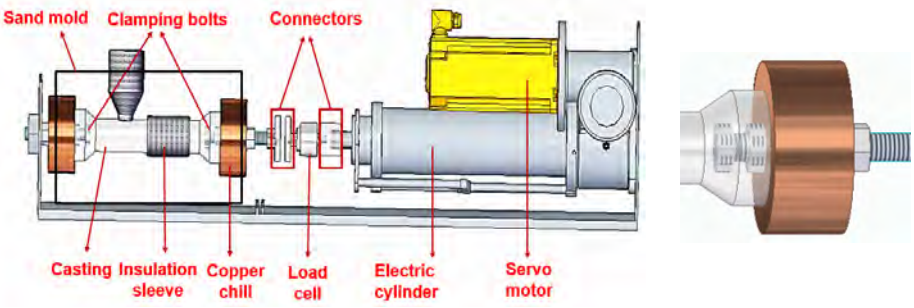

(a) (b)

Figure 6: (a) Schematic of the Controlled Deformation Test (CDT) setup showing the main components of this apparatus, and (b) a detailed view of the attachment between the clamping bolts and the copper chill.

All of the components were placed on a custom-made platform, as shown schematically in Figure 7. The electric cylinder, servo motor and drive were fixed to the platform. A protective steel plate was used between the sand mold and the electric cylinder to protect the device. A steel flask was used as the “mold box” to keep the sand mold rigid and to support the copper chills.

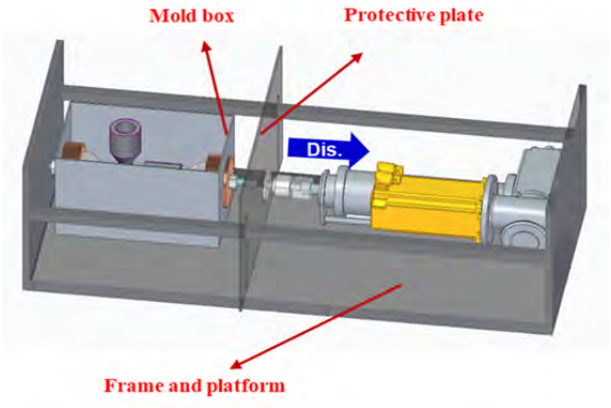

Figure 7: The controlled deformation test setup shows how the mold box and electric cylinder were attached to the steel frame, and the blue arrow in the picture indicates the direction of the movement of the electric cylinder.

Test procedure

Two different types of experiments were carried out in this study to check the capabilities of the test setup and optimize the test parameters. For both tests, a common medium carbon steel with target composition of 0.25 wt%. C - 0.3 wt%. Si – 0.5 wt%. Mn – 0.035 wt%. P – 0.03 wt%. S were used. For each test, before testing, a no-bake sand mold was prepared separately in the mold box, and then placed in the proper position on the platform. Figure 8(a) shows the experimental setup assembly; Figure 8(b) shows a close view of the LVDT and load cell. LabView software was used to control the movement of the motor. Additionally, LabView data acquisition input modules were connected to the LVDT and the load cell to collect and record the displacement and force data as a function of time.

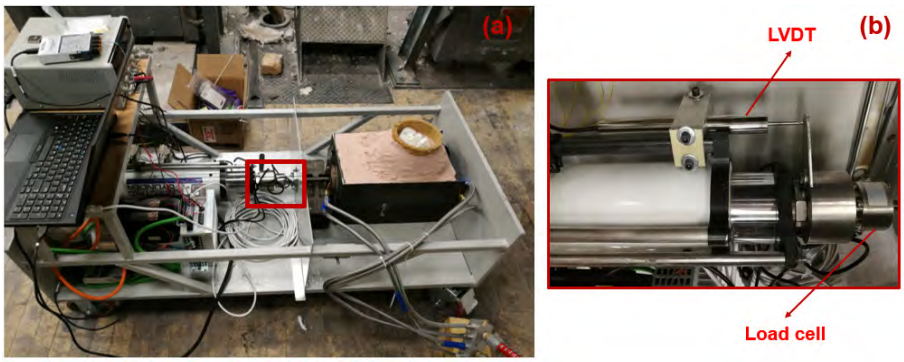

(a) (b)

Figure 8: (a) Assembly of the experimental setup, and (b) detail view of the position of the LVDT and load cell.

High purity induction iron, ferrosilicon, electrolytic manganese and cast iron were melted in a coreless 100 lbs capacity induction furnace under argon cover with a flow rate of 45 SCFH. The cast iron served as a source of carbon. When there was a small liquid pool was observed, the pyrite powder was added into the furnace as the source of sulfur. The molten metal was tapped at 1650 °C into a teapot ladle and killed by 0.05 wt.% high purity aluminum shots in the ladle. Then the liquid metal was poured into the sand mold at 1550°C in 5~6 s. At the same time, the force and displacement changes were monitored in the computer. Before the start of the deformation test, to avoid any premature deformation in the casting, the solidification contraction was compensated for by slowly moving the electric cylinder to maintain zero force reading on the load cell. After a specified amount of time, the casting was pulled by the electric cylinder at a constant strain rate. In the first test (Test 1), multiple deformation steps were applied during the test and the casting was totally fractured after the test. A 4% strain was used at each deformation step in this test and the strain rate was $5*10^{-3}$ /s. In the second test (Test 2), the test was stopped immediately after a load drop or a load deviation was observed on the load cell readings, which indicates the yield or failure of the material. The strain rate in Test 2 was 10^{-3} /s. These two tests varied the test start time. For Test 1, the test start time was 300 s after pouring. For Test 2, it was 480 s after pouring. The test start time was selected based on the MAGMASOFT solidification analysis of the steel. More details about how to determine the test start time will be discussed in the following section.

RESULTS AND DISCUSSION

Thermodynamic modeling

To determine the test start time after pouring, the solid fraction vs temperature curve for the current steel grade (0.25 wt%. C - 0.3 wt%. Si – 0.5 wt%. Mn – 0.035 wt%. P – 0.03 wt%. S) was calculated using the Schiel solidification model in FactSage (Version 7.1) thermodynamic software. Figure 9 shows the calculated solid fraction as a function of temperature. The liquid impenetrable temperature (LIT), which is considered the point below which the dendrites are connected enough to resist the feeding of the interdendritic liquid [4] [21], has been shown to correspond to a solid fraction of 90% [22-23]. Therefore, from the solid fraction – temperature curve, the LIT for the steel composition of interest was determined to be 1420 °C for the current steel composition.

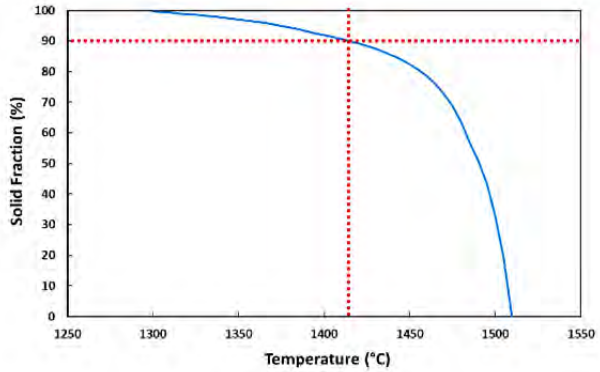

Figure 9: Calculated solid fraction and temperature curve for the studied steel by Scheil equation, which was used to estimate the LIT (dotted lines).

Casting solidification simulation

Figure 10 shows the results of the solidification simulation using MAGMASOFT. Figure 10 (a) shows the predicted fraction of liquid at 6 minutes after solidification. It should be noted that the two sides of the casting were fully solidified because of the water cooled copper chills while the area within the insulation sleeve (short for insulated area) was only partially solidified. A cross section view of solid fraction the insulated area is shown in Figure 10 (b) and this reveals that a uniform solid shell was predicted to form in this area.

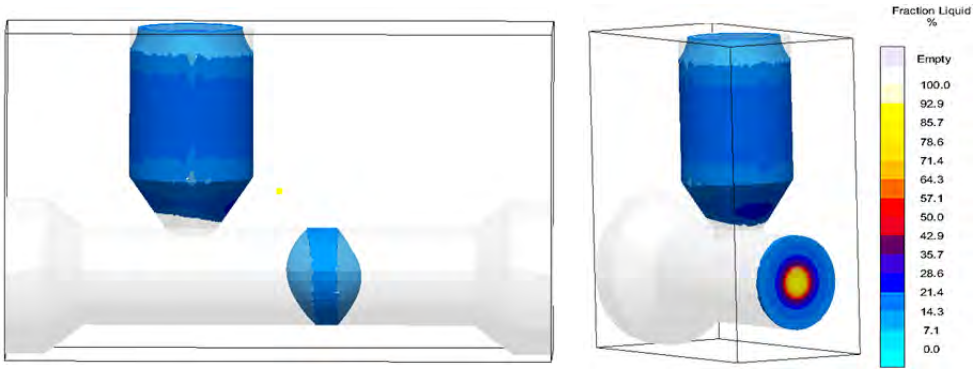

(a) (b)

Figure 10: MAGMASOFT solidification modeling shows (a) the solidification sequence of the casting and (b) the cross sectional view of liquid fraction in the insulated area.

The last solidified cross section in the casting was near to the center of the insulated part of the casting, based on the solidification simulation. To establish relationship between the temperature and time, the temperature at two fixed locations within the last solidified cross section was predicted, as shown in Figure 11 (a). One predicted temperature was in the center of the casting and another one was in 10mm radial position from the surface. Figure 11(b) shows the simulated temperature history of these two points. Test 1 was aimed to check the accuracy of the setup and examine the structure of the fracture

surface, so the test start time was decided as 300 s to make sure there still had liquid metal when the start of the test. Test 2 was design to start the test when the solid shell in the insulated area was about 10mm. Thus, when the temperature at the 10mm thickness position is equal to the LIT, the corresponding time is the test start time, which was determined to be 480 s.

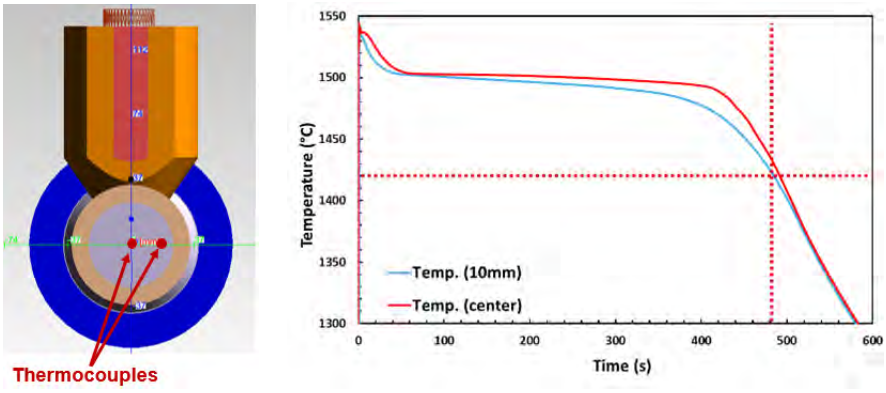

(a) (b)

Figure 11: (a) Cross sectional view of the insulated area with the position of the simulated thermocouples and, (b) simulated temperature history in different positions of the casting.

CDT results

Table 1 gives the target and measured chemistry of the steels employed in the two tests. The main elements were measured by optical emission spectroscopy (OES). LECO* combustion method was used for C, S. The measured compositions were in good agreement with the targeted chemistry. It should be noticed that the measured sulfur was slightly higher than the expected amount, which may have been caused by the segregation of sulfur, since the samples used for measuring the sulfur were cut from the insulated area, which was the last area in the casting to solidify.

Table 1: Measured steel chemistry in two test (wt.%).

Element (wt. %)	Fe	*C	Mn	*S (ppm)	P	Si	Al
Target	Bal.	0.17~0.23	0.3~0.6	300	<0.04	0.3~0.4	0.05
Test 1	Bal.	0.23	0.55	319	0.014	0.38	0.054
Test 2	Bal.	0.20	0.59	353	0.021	0.35	0.045

Figures 12 (a) and (b) show the load and displacement measurements obtained during Test 1 and Test 2, respectively. When pouring the metal into the mold, the liquid metal flow pushed the copper chill, which was connected with the load cell and the load cell measured the resultant compression force. As solidification started, the compression force began to decrease because of solidification contraction and solid section shrinkage. For Test 1, the test started 300s after pouring, which is indicated by the change of the displacement. Four deformation steps were applied to the casting in this test at a constant strain rate of $5*10^{-3}$ /s and each deformation step was at a 4% strain. It should be noted that the amount of strain was calculated using the length of the insulation sleeve as the gauge length. Among these four deformation steps, the last step had the maximum tensile force of about 2.6KN.

For Test 2, before the start of the test, the holding time before applying strain to the casting was longer compared with the waiting time in Test 1 to ensure that a thicker solid shell formed before strain was applied. A larger solidification contraction was observed, which was related to thicker solid shell that formed in the test. To compensate the solidification contraction, a "negative" displacement was applied to keep the measured force near zero. The deformation test started at 480 s after pouring at the strain rate of 10^{-3} /s. The maximum force in this test was around 13KN. Shell deformation was stopped immediately after the first observed load drop.

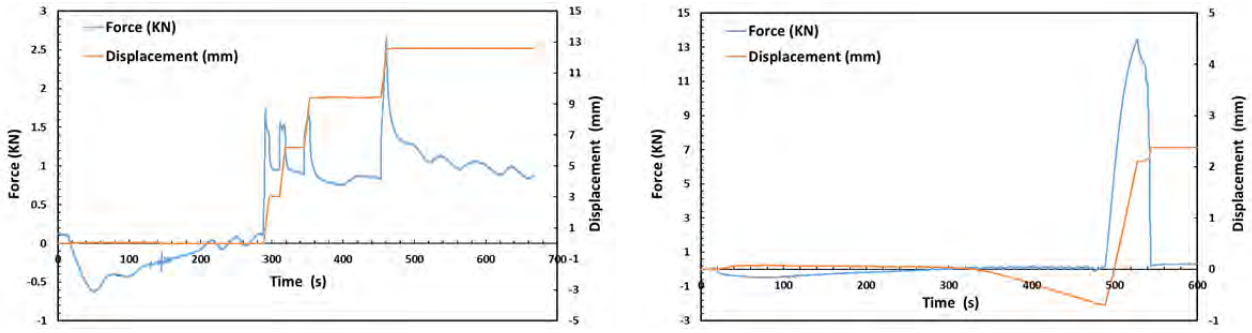

(a) (b)

Figure 12: Load and displacement change during (a) Test 1 and (b) Test 2.

Figure 13 shows the results of the whole test casting, detailing the insulated area after Test 1 and Test 2, respectively. After the Test 1, the casting was totally broken. And the failure position was close to the center of the insulation sleeve, which was expected. For Test 2, some surface cracks were observed on the casting surface.

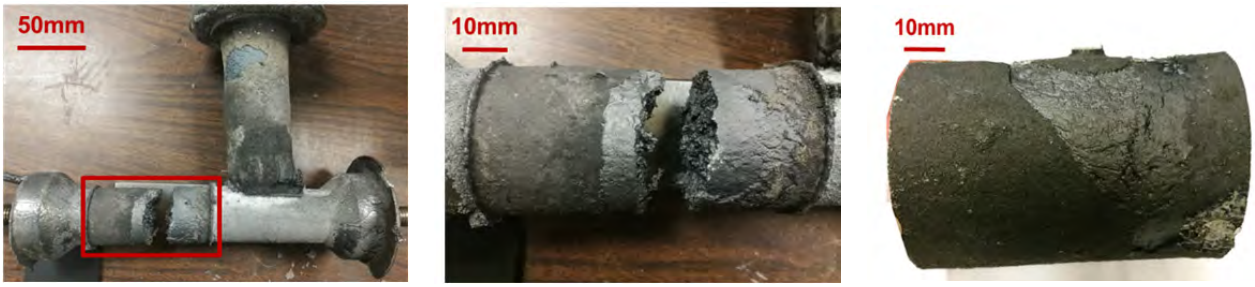

(a) (b) (c)

Figure 13: Results of the casting: (a) Complete casting after Test 1, (b) insulated area after Test 1, and (c) insulated area after Test 2.

An overview of the fracture surface after Test 1 is shown in Figure 14 (a). Columnar structure was observed on the upper side of the surface. On the lower side, there was evidence of liquid flow, which means when the test started, liquid was still present in the center of the insulated part and this liquid flowed to the lower side of the fracture site during the test. Figure 14 (b) shows a closer view of a part of the fracture surface, which was highlighted by the red box in the Figure 14 (a). Figure 14 (b) confirms that the dendrite structures grows from the surface towards the center of the casting in the insulated area, which satisfies with the requirement of the experimental design. Under higher magnification Figure 14 (c), single isolated dendrites can also be observed.

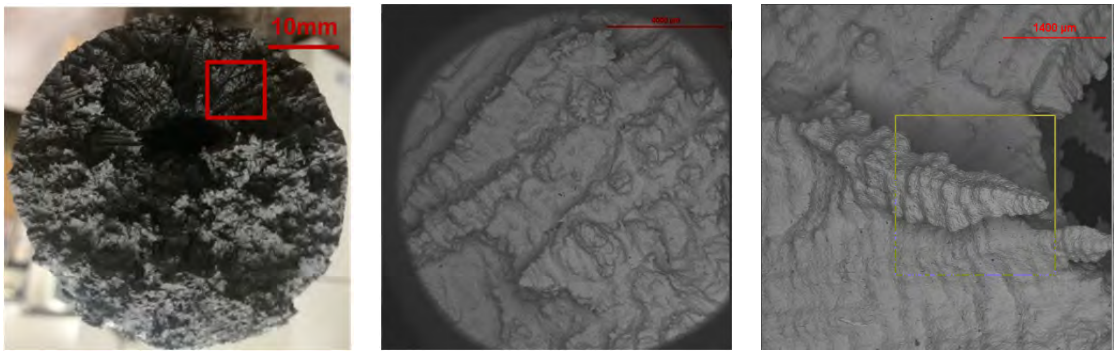

(a) (b) (c)

Figure 14: (a) An overview of the fracture surface after Test 1; (b) zoom of part of the fracture surface to show the growth direction of the dendrites; and (c) higher magnification SEM image to show a signal dendrite structure on the fracture surface.

To observe the internal crack, the insulated part of Test 2 was sectioned in longitudinal direction. Then small specimens were sectioned, mounted and polished for crack observation and chemistry analysis. As shown in Figure 15 (a) and (c), small internal cracks were found to be perpendicular to the direction of the external strain. Figure 15 (b) and (d) show the sulfur distribution in the area of (a) and (c) respectively, which were obtained by ASPEX EDS mapping. It should be noted that in the crack area, the sulfur concentration was higher than other area. It is well known that sulfur has a low partition ratio and it is easy to segregate to the inter-dendritic region, which can flow and accumulate at the crack site as damage occurs [24]. Those low-melting compositions increase the internal crack sensitivity and their enrichment at the crack site serves as a signature of the hot tearing. By comparing the sulfur EDS mapping with the position of the cracks, it can be demonstrated that these internal cracks are the results of hot tearing.

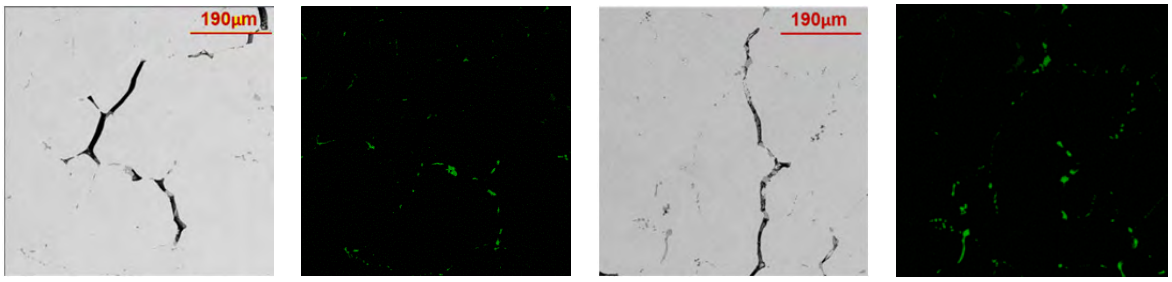

(a) (b) (c) (d)

Figure 15: (a) and (c) Internal cracks that were observed in the insulated part after the test 2; (b) and (d) EDS mapping in the area of (a) and (c) to show the sulfur distribution in those area.

CONCLUSIONS

In the present study, a laboratory method to investigate hot tearing formation in the continuous casting process was developed and tested. For the mold design, two water cooled copper chills and a centrally located low thermal conductivity insulation sleeve were used to control the solidification of the casting. Solidification simulations show that the insulated area is the last area to solidify in the mold. The solid shell grows from the surface towards the center uniformly in the insulated area, which satisfies the experimental requirements to simulate continuous casting shell growth. Two different tests were carried out in the present work. These tests confirm the capabilities of this experimental setup to induce hot tearing under controlled thermo-mechanical conditions. Test results indicate that the experimental setup has the ability to monitor the force and displacement change during the solidification of the casting and successfully create conditions for hot tear formation. A test method to quantitatively evaluate and compare the hot tearing susceptibility for different grades of steel has been demonstrated, and testing on a variety of alloy systems of interest are still ongoing.

ACKNOWLEDGEMENT

The authors would like to thank undergraduate research assistants for their contribution on the sample preparation: Aileen Martinez, Ethan Klafehn, Graham Straley. Acknowledge Brian Bullock for his help with the setup manufacture. This project was supported by Peaslee Steel Manufacturing Research Center (PSMRC) at Missouri University of Science and Technology (Missouri S&T), so special thanks go to all the faculties and industry mentoring committee of PSMRC for their help and guidance. The authors are also grateful to MAGMA LLC for their support to Missouri S&T and their contribution to the simulation work within this project.

REFERENCES

1. Junli Guo and Guanghua Wen, "Influence of alloy elements on cracking in the steel ingot during its solidification," Metals, vol. 9, no. 8, p. 836, 2019.
2. J.-M. D. M. G. M. Rappaz, "A New Hot-Tearing Criterion," Metallurgical and Materials Transactions A, vol. 30A, pp. 449-455, 1999.
3. L. H. Chown, "The influence of continuous casting parameters on hot tensile behaviour in low carbon, niobium and boron steels," University of the Witwatersrand, Johanneshurg, 2008.

4. Young Mok Won, Kyung-hyun KIM, Tae-jung Yeo and Kyu Hwan Oh, "Effect of cooling rate on ZST, LIT and ZDT of carbon steel near melting point," ISIJ International, vol. 38, no. 10, pp. 1093-1099, 1998.
5. Hirowo G. Suzuki, Satoshi Nishimura and Shigehiro Yamaguchi, "Characteristics of hot ductility in steels subjected to the melting and solidification," ISIJ, vol. 22, p. 48~56, 1982.
6. Young Mok Won, Tae-jung Yeo, Dong Jin Seol, and Kyu Hwan Oh, "A New Criterion for Internal Crack Formation in Continuously cast Steels," Metallurgucal and Materials Teansactions B, vol. 31B, pp. 779-794, Aug. 2000.
7. F. P. B. J. A. A. M. Z. Y. L. J. Song, "A Review on Hot Tearing of Magnesium Alloys," Journal of Magnesium and Alloys, vol. 4, pp. 151-172, 2016.
8. J. W. T. Lankford, "Some consideration of strength and ductility int he continuous-casting process," Metallurgical Transactions, vol. 3, pp. 1331-1357, 1972.
9. M. R. Nasresfahani and B. Niroumand, "Design of A New Hot Tearing Test Apparatus and Modification of its operation," Met. Mater. Int.,, vol. 16, no. 1, pp. 35-38, 2010.
10. Stephen Instone, David StJohn & John Grandfield, "New apparatus for characterising tensile strength development and hot cracking in the mushy zone," lnt. J. Cast Metals Res., pp. 441-456, 2000.
11. L. Bichler, C. Ravindran, "New developments in assessing hot tearing in magnesium alloy castings," Materials and Design, pp. 17-23, 2010.
12. H. Z. F. G. S. D. X. T. R. Xu, "A New Investigated Method on Hot Tearing Behavior in Aluminum Alloys," vol. 54, no. 5, pp. 377-382, 2013.
13. Yeshuang Wang , Qudong Wang, Guohua Wu, Yanping Zhu, Wenjiang Ding, "Hot-tearing susceptibility of Mg–9Al–xZn alloy," Materials Letters, vol. 57, pp. 929-934, 2002.
14. G. Cao, S. Kou, "Hot cracking of binary Mg–Al alloy castings," Materials Science and Engineering A, vol. 417, pp. 230-238, 2006.
15. Shuang-Shou Li • Bin Tang • Xin-Yan Jin, Da-Ben Zeng, "An investigation on hot-cracking mechanism of Sr addition into Mg–6Al–0.5Mn alloy," J Mater Sci, vol. 47, pp. 2000-2004, 2012.
16. C. Monroe, C. Beckermann, "Simulation of hot tearing and distortion during casting of steel: comparison with experiments," in SFSA 60th Conf. Proc., 2006.
17. D. S. Bhiogaed, S. M. Randiwe and A. M. Kuthe, "Failure analysis and hot tearing susceptibility of stainless steel CF3M," International Journal of Metalcasting, vol. 13, no. 1, pp. 166-179, 2019.
18. C. Bernhard, H. Hiebler, and M.M. Wolf, “Simulation of shell strength properties by the SSCT test”, ISIJ Int. (Japan), Vol. 36, pp. S163-S166, 1996
19. M. Rowan, B. G. Thomas, R. Pierer and C. Bernhard, “Measuring mechanical behavior of steel during solidification: Modeling the SSCC test,” Metallurgucal and Materials Teansactions B, vol. 42B, pp. 837-851, Aug. 2011.
20. M. Suauki, C. Yu and T. Emi, “In-Situ Measurement of Tensile Strength of Solidifying Steel Shells to Predict Upper Limit of Casting Speed in Continuous Caster with Oscillating Mold,” ISIJ Int., Iron Steel Inst. Japan, Vol. 37(4), pp 375-382, 1997.
21. Dong Jin Seol, Young Mok Won, Kyu Hwan Oh, Yong Chang Shin and Chang Hee Yim, "Mechanical Behavior of Carbon Steels in the Temperature Range of Mushy Zone," ISIL International, vol. 40, pp. 356-363, 2000.
22. M. B. Santillana, "Thermo-mechanical properties and cracking during solidification of thin slab cast steel," Tata Steel Nederland Technology B.V., 2013.
23. M. Rappaz, J.-M. Drezet, and M. Gremaud, "A new hot-tearing criterion," Metallurgical and Materials Transactions A, vol. 30A, pp. 449-455, 1999.
24. Gonzalo Alvarez de Toledo, Oscar Campo and Enrique Lainez, "Influence of sulfur and Mn/S ratio on the hot ductility of steels during continuous casting," Steel Research, vol. 64, no. 6, pp. 292-299, 1993.

